Biophysical Journal Volume 105 August 2013 711–719

Protein-Mediated Transformation of Lipid Vesicles into Tubular Networks

Mijo Simunovic,[†] Carsten Mim,[‡§] Thomas C. Marlovits,[¶‖] Guenter Resch,[¶‖] Vinzenz M. Unger,[‡§] and Gregory A. Voth[†*]

[†]Department of Chemistry, Institute for Biophysical Dynamics, James Franck Institute, and Computation Institute, The University of Chicago, Chicago, Illinois; [‡]Department of Molecular Biosciences and [§]Chemistry of Life Processes Institute, Northwestern University, Evanston, Illinois; [¶]Research Institute of Molecular Pathology, Vienna, Austria; and [‖]Institute of Molecular Biotechnology, Austrian Academy of Sciences, Vienna, Austria

ABSTRACT Key cellular processes are frequently accompanied by protein-facilitated shape changes in the plasma membrane. N-BAR-domain protein modules generate curvature by means of complex interactions with the membrane surface. The way they assemble and the mechanism by which they operate are largely dependent on their binding density. Although the mechanism at lower densities has recently begun to emerge, how membrane scaffolds form at high densities remains unclear. By combining electron microscopy and multiscale simulations, we show that N-BAR proteins at high densities can transform a lipid vesicle into a 3D tubular network. We show that this process is a consequence of excess adhesive energy combined with the local stiffening of the membrane, which occurs in a narrow range of mechanical properties of both the membrane and the protein. We show that lipid diffusion is significantly reduced by protein binding at this density regime and even more in areas of high Gaussian curvature, indicating a potential effect on molecular transport in cells. Finally, we reveal that the breaking of the bilayer topology is accompanied by the nematic arrangement of the protein on the surface, a structural motif that likely drives the formation of reticular structures in living cells.

INTRODUCTION

Remodeling of cellular membranes is intimately associated with many biological phenomena. This process is possible due to a highly dynamic relationship between proteins and lipids, which allows membranes to form an impressive variety of shapes to divide, migrate, communicate with other cells, initiate organelle biogenesis, and enable trafficking (1,2). Recent progress in experimental and theoretical methodologies has allowed us to understand the way proteins sense and generate curvature and thus form crucial parts of the complex cellular machinery (3). The membrane remodeling superfamily of Bin/Amphiphysin/Rvs (BAR)-domain proteins has been implicated in many important cellular tasks, most notably clathrin-mediated endocytosis (4–6). They are best known for their preferential binding to curved membranes and their ability to form and stabilize membrane tubules (7–11). These crescent-shaped proteins contain variable modules, wherein the BAR domain is responsible for their membrane-bending function (7). It is important to note that their functional variability arises from the difference in shape of BAR domains. Although the magnitude of intrinsic curvature of these domains is not directly imprinted on the lipid bilayer, in complex ways it determines the final shape of the membrane. F-BAR proteins (such as FCHo2) are characterized by having the lowest positive intrinsic curvature, thus inducing the formation of tubules of large diameters (60–100 nm) (11). BAR/N-BAR-containing proteins (such as endophilin, amphiphysin, centaurin, and sorting nexins) induce a higher curvature when binding to the membrane, with tube diameters measuring from 20 to 60 nm (7,12). Conversely, I-BAR proteins (e.g., missing in metastasis) induce negative curvature resulting in membrane invaginations (viewed from the protein) (13).

Most BAR protein dimers contain two or more amphipathic helices at their N-termini. The shallow insertion of this structural motif into the bilayer is thought to be a key mechanism in curvature generation, complementing ionic interactions between the membrane and the proteins (14). Recent experiments imply that BARs have a more involved role than just shaping the membrane, since proteins containing amphipathic helices induce appreciable vesiculation (15,16). This finding implicates N-BAR proteins, and especially endophilin, to have a role in membrane fission. At the same time, experimental and theoretical reports have provided important insights into the physical mechanism underlying N-BAR-induced membrane remodeling. Fluorescence microscopy revealed two distinct mechanisms that depend on the bound density of the protein (17). In the low-density regime (<4% bound density) proteins do not interact, and their mode of action is only sensory. Conversely, at higher densities, the results suggested that proteins aggregate and even form lateral scaffolds on the membrane tubes (9). Recent simulations have revealed a surprising mechanism of curvature generation at densities up to ~20% (M. Simunovic, A.S., and G. A. Voth, unpublished). It was shown that highly anisotropic interactions between N-BAR proteins and the surface of the membrane lead to curvature-driven linear aggregation of proteins. This process induces budding of the membrane, with the protein molecules mostly concentrated in the necks of

Submitted May 2, 2013, and accepted for publication June 28, 2013.

*Correspondence: gavoth@uchicago.edu

Editor: Gerhard Hummer.

0006-3495/13/08/0711/9 $2.00

http://dx.doi.org/10.1016/j.bpj.2013.06.039

emerging buds. Considering the complexity and the seemingly disparate nature of the published experimental evidence, the precise role of BAR proteins in each step of endocytosis and the full extent of their remodeling capabilities is still a matter of active research.

The sheer scale of dynamic biological phenomena such as protein-induced membrane remodeling demands a multidisciplinary approach. Here, we combine coarse-grained (CG) molecular dynamics (MD), mesoscopic quasiparticle simulations of vesicles, and electron microscopy (EM) to study membrane remodeling under the high-density regime of N-BAR proteins. CG MD simulations provide insights into the remodeling dynamics at molecular resolution, thus allowing the observation of protein assembly and the mobility of lipids in the course of the reshaping (18,19). Mesoscopic simulations, on the other hand, access much larger time- and lengthscales, necessary for a systematic analysis of the quasiequilibrium remodeled structures under varying conditions (20,21). Finally, EM imaging provides qualitative clues into the consequences of protein-membrane interactions at very long timescales in vitro (9). In our previous work, we reported the formation of complex tubular structures induced by endophilin, although the work at the time was limited to a qualitative description (20). Here, we present what is to our knowledge a novel N-BAR remodeling phenomenon in which the proteins induce a reticulation of lipid vesicles into a network of interconnected tubules. We describe the shape changes of vesicles upon binding of proteins at both molecular and mesoscopic resolutions. Additionally, we quantify the mechanical effect of high-density binding on the membrane and its effect on lipid mobility. Finally, we propose a mechanism for the observed vesicle transformation.

MATERIALS AND METHODS

MD simulations

A previously developed three-site hybrid CG model was used for the lipid bilayer (22). The modeling combines forces from the bottom-up multiscale CG method with analytical functions to cover poorly sampled regions of the configurational space (22–24). The forces between lipids were used in a tabular form with a 2 nm cutoff distance. A 26-site N-BAR-domain model was used with intraprotein interactions modeled as harmonic bonds (9), whereas protein-protein and protein-lipid interactions were modeled with a Lennard-Jones potential (25). The Lennard-Jones parameters used were 1.8 kcal/mol well depth at 1.5 nm between sites representing amphipathic helices and lipid headgroups, 0.2 kcal/mol at 1.5 nm for other protein sites and the lipid headgroup, and 0.24 kcal/mol at 2 nm for all protein-protein interactions. These parameters were derived by combining previous free-energy simulations (25) and the binding energy from fluorescence experiments (17). For simulations of transformations of vesicles, we coated a spherical vesicle with N-BAR proteins at 10%, 50%, and 90% coverage. The simulations were carried out under constant *NVT* conditions (*V* being the volume of the simulation box), with the thermostat set to 300 K (coupling constant, 6τ, $\tau = 49$ fs). Configurations for reticular liposomes were recreated from mesoscopic simulations as previously described (26). In the procedure, the surface of the membrane was triangulated with vertices lying at membrane quasiparticles. The triangulated regions were then filled with patches of preequilibrated CG membrane. Subsequently, the recreated CG membrane was coated with CG proteins to the desired surface density. Simulations were carried out at four surface densities: 0%, 50%, 90%, and 95%. All simulations were run for 2–6 million CG time steps with a time step up to 0.4τ in the LAMMPS (27) MD package.

For lateral pressure calculations, the stress tensor was rotated into a reference frame with the z' axis parallel to the membrane normal and the x' axis parallel to the principal direction of curvature. The components of the stress tensor ($\sigma_{a=x,y,z}$) were calculated with LAMMPS. The normal and principal vectors were calculated using the maximum entropy approach (28). The volume (V) was approximated with a double tessellation method as $A^{3/2}$. Finally, the lateral pressure on lipid i ($p_{\mathrm{lat},i}$) was calculated according to Eq. 1,

$$p_{\mathrm{lat},i} = -\frac{1}{V_i}\left(\sigma_{z'} - \frac{1}{2}\left(\sigma_{x'} + \sigma_{y'}\right)\right)_i \tag{1}$$

Lipid diffusion rates (D) were calculated from 3D mean-square displacements, according to Eq. 2. For overall lipid diffusion rates, the value was averaged over all lipids in the system, whereas for calculations of diffusions of confined lipids, a cutoff distance of 1.5–2.5 nm (from either the protein or a point on a membrane) was used.

$$D = \frac{1}{6t}\frac{1}{N_{\mathrm{cut}}}\sum_{i}^{N_{\mathrm{cut}}}\left\langle\left(\mathbf{r}_i(t) - \mathbf{r}_i(t_0)\right)^2\right\rangle \tag{2}$$

It must be noted that the timescale of CG MD simulations is not well defined relative to real (actual) time given the degrees of freedom eliminated in going to the CG model. Therefore, in this work, relative diffusion rates, and not absolute rates, are compared.

Mesoscopic simulations

The details of the model and the simulation method can be found elsewhere (20,21). Briefly, the elastic continuum membrane is discretized into quasiparticles and immersed into a mesoscopic solvent. The discretization allows for large-scale restructuring, thermal fluctuations, and a more flexible computational approach. Each particle has superimposed a field variable describing the composition of proteins, whereas membrane particles have additionally superimposed the composition of lipids. Composition field variables are molar fractions of 1), N-BAR proteins and 2), negatively charged lipids, ranging from -1 to 1 (representing 0% and 100%, respectively). The motion of particles is controlled with smooth-particle applied mechanics (29), where the composition field variable evolves according to the Landau-Ginzburg equation (30). The initial composition on each particle was randomly assigned from -1 to 1, except for particles inside the vesicle, where the protein concentration was set to zero. The effect of the protein on the membrane is modeled through a composition-dependent bending modulus (local stiffening induced by the protein) and by coupling the local membrane curvature with the spontaneous anisotropic curvature (c_0^{-1}) generated by the protein. Nematic protein assembly may be favored by including an additional oligomerization parameter. We demonstrate later that the vesicle transformation occurs even in the absence of this parameter but may facilitate tubule formation for lower intrinsic curvatures (20). The total energy is thus a sum of membrane bending energy, energy arising due to changes in lipid and protein compositions, the interaction energy between the membrane and the protein, and oligomerization energy. All simulations were carried out at 300 K, starting from spherical liposomes, with a lengthscale of each quasiparticle in the range 5–10 nm.

Protein purification and liposome preparation

Rat endophilin A1, rat amphiphysin 1, and the N-BAR domain of rat endophilin (amino acids 1–247) were purified as previously described (9). In all

experiments, synthetic lipids were used (Avanti, Alabaster, AL). The various lipid mixtures prepared were (w/w) 80% dioleoylphosphoserine, 20% dioleoylphosphocholine (for remodeling with endophilin N-BAR EM cryotomograms), 50% dioleoylphosphoserine, 45% dioleoylphosphoethanolamine, and 5% cholesterol (in all remodeling assays). The large unilamellar vesicles were synthesized as before (9). Liposomes (0.1–0.25 g/L) were equilibrated at room temperature before adding the protein at a lipid/protein (w/w) ratio of 1.4:1 (endophilin, endophilin N-BAR) or 1:1 (amphiphysin).

EM imaging and image processing

Negative stain images were recorded using samples stained with 1% uranyl acetate with Tecnai 12 microscope (FEI/Philips, Eindhoven, The Netherlands) at 120 kV. Images of unstained samples were acquired at a temperature of −170°C with a Tecnai F20 Twin transmission electron microscope at 120 kV. Images were recorded with a Tietz F415 4k × 4k pixel CCD camera using the Leginon data collection software (31) at nominal magnifications of 29,000 and defocus values of −1.5 μm to −2 μm. Electron cryotomography was performed on an FEI F30 Polara (FEI/Philips, Eindhoven, The Netherlands) and Gatan 4k × 4k pixel CCD camera. The images used in the figures were contrast-enhanced to increase visibility of fine molecular features. Tomograms were reconstructed and segmented with the IMOD package (32). Visualization of EM images and optical density analysis was performed with ImageJ (33).

RESULTS AND DISCUSSION

Very high bound density of N-BAR domains induces a topological transformation of a lipid vesicle

In tubulation assays, the interaction between N-BAR-containing proteins and lipid vesicles leads to the formation of tubules that grow in the orientation of the protein bound to the lipid surface (7,8,17). This process is generally depicted as a transformation in which the tubules continuously emerge from the membrane. We previously observed the formation of a series of seemingly connected tubules when incubating N-BAR proteins with large liposomes (20). Although it was not apparent from EM imaging at the time, our mesoscopic simulations suggested that these morphologies could be obtained via the topological breaking of the bilayer structure. To understand the structural and physical properties of membranes after N-BAR binding at the molecular level, we carried out CG MD simulations of infinite flat membrane sheets composed of CG lipids coated with high densities of N-BAR domains. It has been shown (M. Simunovic, A. S., and G. A. Voth, unpublished) that at up to ~20% surface-bound densities, proteins induce the formation of membrane-bud-like structures. At this density regime, the average bending energy per lipid linearly increases, whereas above 20% it remains constant. This surprising finding indicates that in addition to density-dependent remodeling found for very low (<4%) and intermediate densities (10−30%), lipid membranes show distinct morphologies and behavior at high densities of bound N-BAR proteins. Previously published experimental evidence (15) and the aforementioned CG simulations suggest that N-BAR proteins induce buds with diameters almost an order of magnitude larger than the size of the protein. Since the energetic cost of forming a vesicle bud is on the order of $8\kappa\pi$, (κ being the bending stiffness), bud formation on a typical lipid membrane would require an energy of 250 k_BT. A membrane patch that can accommodate a typical N-BAR-induced bud is approximately two orders of magnitude larger in area than the single protein (4000 nm^2 in our simulations). Assuming that the binding energy of N-BARs to the membrane is 10 k_BT (17), overcoming that predicted cost would be equivalent to a coverage of ~25%. Our current simulations at higher densities suggest that steric clashes between proteins inhibit further bending (Fig. 1 *A*, *inset*). The large excess interaction energy at these concentrations may thus be used to compress the membrane and overcome the hydrophobic forces keeping the bilayer topology intact.

The lateral pressure profile around the protein reveals insights into the stretching dynamics of the membrane (Fig. 1 *A*). As previously reported, when the density is low enough that the proteins do not interact (<4%), the bilayer

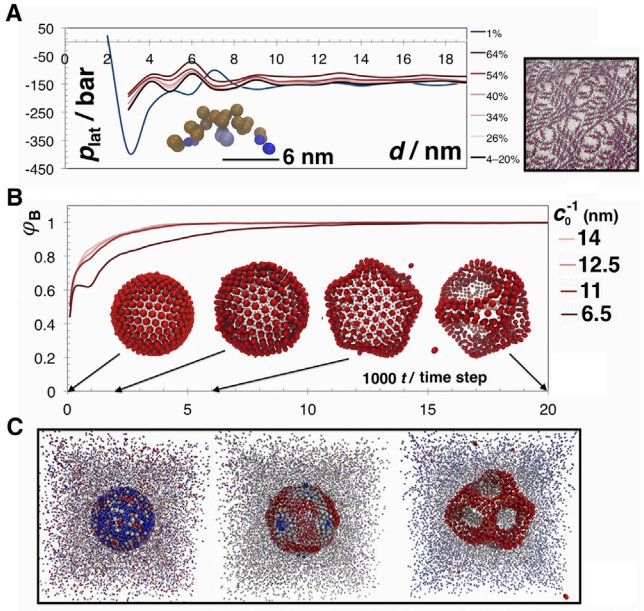

FIGURE 1 Topological transformation of lipid vesicles induced by N-BAR proteins. (*A*) Average lateral pressure profile (per lipid) as a function of the distance from the center of mass of the protein (*d*). (*Right inset*) crowded surface of the membrane at 55–60% protein coverage. (*Bottom inset*) CG representation of an N-BAR domain (*blue*, amphipathic helices). There were no lipids at $d < 3$ nm of the protein's center of mass. (Values for 1–20% were taken from M. Simunovic, A. S., and G. A. Voth (unpublished)). (*B*) The evolution of the protein density field variable during the course of four mesoscopic simulations initiated with different spontaneous curvatures, c_0^{-1}. The variable ϕ_B represents the molar fraction of the protein on the quasiparticle. (*C*) The migration of the N-BAR protein from the solvent to the vesicle (*blue*, low protein density; *gray*, intermediate protein density; *red*, high protein density). Snapshots were taken at 0 (*left*, ϕ_B = ~10%), 2000 time steps (*middle*, ϕ_B = ~80%), and 20,000 time steps (*right*, ϕ_B = ~98%).

is strongly locally constricted. Analytical calculations predict that higher densities should alleviate the stress imposed by a single protein molecule (34). Our simulations confirmed this prediction, showing that at 20% coverage, aggregate formation alleviates membrane stiffening by 150 bar/lipid. The very high-density regime (~65%) further alleviates the absolute maximum pressure, but only moderately (by 50 bar/lipid) compared to the low-density regime (Fig. 1 *A*).

In light of our observations, we consider two possible remodeling mechanisms for membrane tubule formation: 1), continuous tubulation, and 2), topological vesicle transformation. In the former, local linear aggregation and the formation of meshes induce convex budding on the surface of the membrane. The accumulation of the protein starts at the neck of the forming bud and, as additional proteins bind, they coat and elongate the extending tubule (9,15). On the other hand, when the protein covers large portions of the membrane surface, it impedes continuous transformation and, instead, breaks the bilayer topology.

A combined analytical theoretical and experimental study predicts that amphipathic helices are key elements of membrane fission (15), so one may expect endophilin (containing four helices) to more efficiently reticulate the vesicle than amphiphysin (containing only two). In our experiments, both endophilin and amphiphysin were able to form tubular networks, with no appreciable difference in the structure of reticular liposomes (Fig. S1 in the Supporting Material). Apparently, two amphipathic helices in the N-BAR domain are sufficient for binding to high coverage and for subsequent fission. In addition, we confirm that the protein does not require other domains for reticulation, as an isolated N-BAR domain from endophilin efficiently transforms the vesicles (Fig. S1, *left*).

There are two conceptual barriers to understanding the binding of N-BAR proteins at sufficiently high densities to promote topology breaking. 1), Given that the N-BAR domains are highly charged, how can they overcome the strong electrostatic repulsion to cover most of the vesicle surface? It is known from experiments with lipid vesicles that binding of charged colloidal nanoparticles never leads to the maximum coverage (35). Further binding is prevented by either the repulsion of bound colloids or the formation of charged domains serving to neutralize their counterions (36). In our experiments, we overcome this problem by using high charge (>50% phosphoserine lipids), which increases the effective binding affinity of the protein. 2), How can a topological transformation take place if initial binding triggers a continuous tubulation of the membrane? It would be necessary for the proteins to bind faster than membrane remodeling. In our mesoscopic simulations (20,21), we traced the evolution of the composition field variable (i.e., local protein molar fraction) as it migrates from the solvent to the liposome. Topological remodeling occurred (Fig. 1 *B*) after the protein composition on the membrane reached an average of >90%. Strong binding (>80%) is already achieved in 2000 simulation time steps. By 6000 time steps the vesicle begins to remodel, forming a fully reticular structure at 20,000 time steps. These simulations reveal that during the initial binding, proteins rapidly aggregate (Fig. 1 *C*, *middle*). The long linear aggregates observed at initial stages of our simulations are in agreement with curvature-driven self-assembly observed in our CG MD simulations at lower bound densities and to studies of vesicle-particle systems (37). After aggregation, the rapid full binding leads to a topological change and an increased density of the protein in the vicinity of the vesicle (Fig. 1 *C*). Recent simulations of anisotropic curvature inclusions on a triangular membrane model (38) resulted in tubular aggregates similar to those in this study (Fig. 1 *C*, *middle*), which in that case led to continuous tubulation, albeit at lower bound densities. Considering that such models preclude the breaking of the membrane, topological transformations could not have been observed.

The dynamics of the transformation of a lipid vesicle into a continuous tubular network

To study the morphology of the reticular liposome, we carried out CG MD simulations of spherical vesicles 200−300 nm in diameter, which are at least an order of magnitude larger than the protein's intrinsic curvature. To evaluate the effect of protein density on the mechanism of membrane remodeling, we initially coated 10%, 50%, and 95% of the surface with N-BAR proteins. At 10% density, linear aggregation occurred as previously described. We used the trajectories of this system for subsequent diffusion calculations (see next section). At 50% protein density, the vesicle exhibited low-frequency undulating motions suggestive of structural instabilities. In addition, long lateral tubular domains and large buds were formed on the surface (Fig. 2 *A*). Similar to what we observed in flat sheet simulations, steric restraints prevented the N-BAR proteins from forming meshes, precluding the emergence of perpendicular buds that we observed in lower-density simulations. Early in the simulation, there was temporary poration of the bilayer that quickly healed before the undulations began. The formation of pores may be explained as a consequence of temporary reduction in the area/lipid, which is subsequently compensated by opening pores before the vesicle volume can be adjusted. In this regime, the binding energy appears to be too low to induce permanent topological changes in the membrane. By contrast, in simulations with N-BAR density at >90% coverage, the vesicle underwent a lasting topological change. First, pores form rapidly across the surface of the vesicle (Fig. 2 *B*, *1* and *2*). These pores then serve as folding sites where the membrane bends into tubules (Fig. 2 *B*, *2* and *3*). Finally, significant line tension along the region of the topological break, together with the energy from protein binding, leads to the formation of

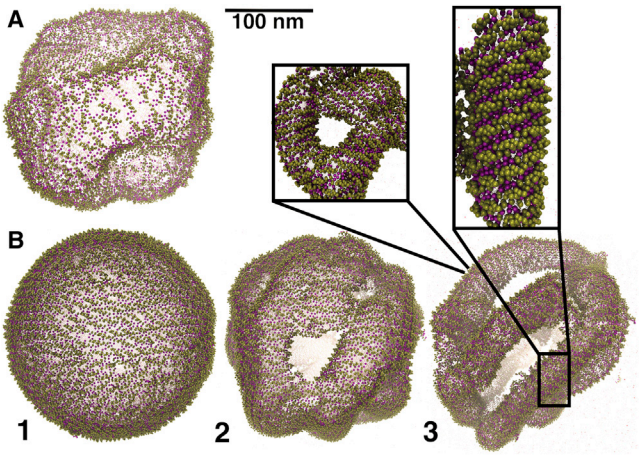

FIGURE 2 Vesicle remodeling under the high-density regime of N-BAR proteins in CG MD simulations. (*A*) Instabilities and lateral tubulations induced by proteins at 50% coverage. (*B*) Reticulation induced by the protein at 90% coverage as a sequence in time. Insets depict the highly aligned assembly of the protein at a tubular junction and on the tubule. The scale bar does not refer to the structures magnified in the inset.

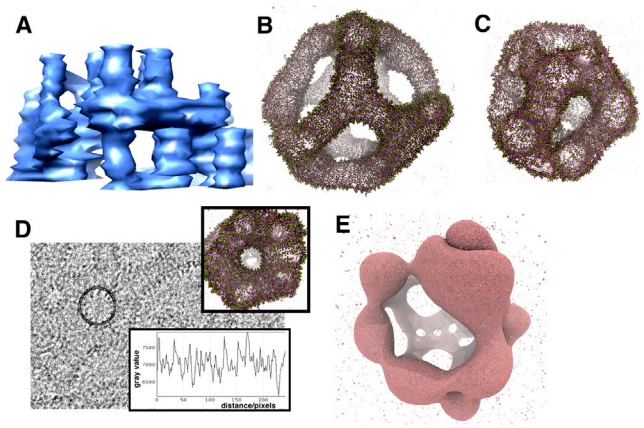

FIGURE 3 Structure and dynamics of the reticular liposome. (*A*) Cryo-electron tomography of the N-BAR-coated tubular network (segmentation of the cryo-EM tomogram). (*B*) CG MD simulation of the molecular reconstruction of the reticular liposome coated with 90% protein density. (*C*) CG MD simulation of the molecular reconstruction at 50% protein density. The structure depicts widened and shorter tubes. (*D*) Optical density plot revealing the alignment of N-BAR proteins on a junction similar to that found in CG MD simulations (*inset*). (*E*) CG MD simulation of a reticular liposome with all N-BARs removed. The vesicle undergoes pearling instabilities.

a closed-surface reticular vesicle. The trajectories from both CG MD and mesoscopic simulations show that reticular liposomes form by a topological change rather than by a continuous transformation of the membrane. In addition, both simulations show a comparable number of intertubular junctions (~10 for a 200 nm vesicle), and the tube diameters (ranging between 15 nm and 25 nm, average ~17 nm) are in agreement with EM images (Fig. S1). From a molecular point of view (CG MD simulations), the protein molecules strongly align during tubule formation, with an angle of ~60° between the main axis of the protein and the axis of the tube (Fig. 2 *B*, *3*, *inset*). This structural arrangement agrees well with previous fluorescence microscopy, EM imaging, and CG simulations (9,17,39), demonstrating that protein scaffolds stabilize long membrane tubules. Our simulations starting from spherical vesicles indicate that these highly static protein arrangements form during membrane breaking and before the formation of the tubules (Fig. 2 *B*, *2*). In contrast to the static local protein structure, mesoscopic simulations show that the reticular structure itself is highly dynamic at longer timescales. The tubules continuously change size, detach from junctions, and rejoin, forming new tubules.

To verify our hypothesis that the EM images represent 2D projections of tubular networks, we carried out a 3D reconstruction of cryotomograms of transformed vesicles. To facilitate the reconstruction, we incubated vesicles with only the N-BAR domain of endophilin, analogous to our CG MD simulations. The tomogram (Fig. 3 *A*) confirms that vesicles comprise a series of interconnected tubules. It is interesting that both planar and spherical subdivisions coexist in the reconstructed structure, consistent with the simulations. Within the planar section, the junctions are spaced evenly, indicating that, as seen in CG MD simulations, these arrays may precede the interconnected tubular structure (Fig. 3 *A*).

Despite the fast transformation, the full maturation of formed tubules into a steady-state closed surface structure is computationally a very slow process (in experiments it occurs on the order of seconds), requiring well beyond the 10 million CG time steps in our simulations. For this reason, we recreated final reticular structures at molecular resolution by mapping CG lipids onto the final configuration of a mesoscopic membrane model (26). Consequently, we effectively achieve the molecular resolution of the membrane remodeling process at experimental timescales.

During the course of the CG MD simulation of the reconstructed reticular liposome, the morphological features and the integrity of the CG reticular vesicle remained unchanged, with the tube diameter staying in the same range, averaged to ~20 nm. N-BAR proteins appear to specifically align in the junction regions, characterized by pronounced Gaussian curvature (Fig. 3, *B* and *C*), likely arising from the highly anisotropic interactions between the protein and the membrane. Complementary to our simulations, the electron micrographs of the reticulated liposomes show striated patterns along these junctions (Fig. 3 *D*). The radial distribution of the optical density in these junction regions showed that the spacing between proteins is 5.1 ± 1.9 nm, in good agreement with the spacing seen on N-BAR-coated tubules. This observation, together with our CG MD simulations, is strong evidence that N-BAR domains exist as multimeric (nematic) assemblies at high-density binding.

The homogenous coverage of proteins could be a consequence of steric interactions, although such interactions would not necessarily lead to aligned protein assemblies. To test the effect of protein density on the morphology of the tubular network and its assembly, we carried out a CG MD simulation starting with the reticular structure at ~50% coverage. In the course of the simulation, the tubules widened to diameters of 19–29 nm, with an average of 24 nm (Fig. 3 *C*). The effect of protein density on tube radius is in excellent agreement with microscopy experiments (17). Interestingly, our simulations show that while the tubes are no longer fully coated at these lower protein concentrations, the proteins still fully cover tubular junctions (Fig. 3, *C* and *D*). Next, we studied the evolution of the reticular liposome with all the N-BAR proteins removed. In the absence of the protein, the structural integrity of the reticular liposome becomes compromised. The tubes widen to 30–70 nm in diameter, leading to pearling instabilities and tube buckling, with the size of individual pearls measuring 30–80 nm (Fig. 3 *E*). In reality, we suspect that spontaneous detachment will occur at very long timescales, considering the high binding constant and the slow unbinding rate of N-BAR proteins (17).

Protein binding and remodeling affect lipid diffusion rates in a density-dependent manner

Localization of transmembrane and membrane-associated proteins is dependent on lateral diffusion, implying that factors influencing the mobility of lipids may play an important role in biological processes (40–44). It has been shown that in areas of high curvature, the diffusion rate of lipids in bilayer membranes is reduced (42). In addition, changes in membrane density, especially crowding, have a marked effect on lipid lateral dynamics (43,44). Given the interesting morphology of our system, it is valuable to investigate how protein binding and aggregation and membrane remodeling affect lipid mobility in CG simulations. Although in principle we would like to determine lateral diffusion of lipids, in practice it is difficult to define this value in highly remodeled systems. We analyzed simulations of spherical and reticular systems by measuring the mean-square displacement of lipids under various conditions and calculating their 3D diffusion rates. Considering that it is not known how the dynamics in CG simulations compares to real dynamics, we compared the calculated diffusion rates to the mobility of lipids in simulations of an unbound liposome.

At low densities of bound N-BARs (~10% coverage), the average lipid mobility is somewhat attenuated (0.90 times the value of free lipids) (Table S1 and Fig. S2). The diffusion rate of lipids around the protein is only moderately reduced from the overall diffusion at this density (0.88 times the value of free lipids), most likely due to the presence of local regions of increased curvature induced by the proteins. At high densities (~50%), the overall lipid diffusion rate is decreased by 20% compared to that of free lipids. The decrease is even more pronounced for lipids interacting with the protein, which diffuse 35% more slowly than the reference value. Considering that beyond 20% bound density, the average curvature of the system remains constant (therefore not a curvature effect), the binding of N-BAR proteins at high densities directly affects the fluidity of the membrane. This observation complements the pressure analysis, in which a stiffening of the membrane was observed in the presence of the protein, both contributing to the breaking of the bilayer topology.

To further differentiate between the effects of protein binding and membrane curvature, we measured the mobility of the proteins in geometrically confined areas of the membrane. The diffusion rates of tubular lipids not interacting with the protein were reduced by 33%, quantitatively in striking agreement with the experimentally measured reduction of 33–40% (42). The diffusion rate of tubular lipids in direct contact with the N-BAR proteins was reduced even further to 60% of the reference value. Furthermore, lipid motion is highly hindered in domains of high Gaussian curvature (Fig. 3, *D* and *E*), with the average diffusion rate dropping to 40% of the reference value. Such curvatures are found in many areas of the cell, specifically at the base of endocytic buds where the dynamics of proteins is especially complex during signal transmission among neurons.

These results illustrate the complex interplay between protein binding and membrane remodeling in determining the rate of lipid diffusion and the associated biological functions. Perhaps surprisingly in all density regimes the difference between the reference diffusion rate and the overall average rate of lipid diffusion is larger than the difference between the average rate of diffusion and the rate for lipids directly interacting with the proteins. This suggests that membrane curvature is a more direct determinant of lipid mobility than is protein binding or aggregation, an effect that seems to be maximized in the case of regions of high Gaussian curvature.

The transformation of vesicles into a tubular network is defined by a narrow phase space

To understand the precise set of conditions that leads into the formation of tubular networks, we carried out a series of mesoscopic simulations, altering variables controlling the mechanical properties of the membrane, structural and physical parameters of the protein, and the way the two interact. We tested the following parameters: 1), bending stiffness (5–50 k_BT); 2), intrinsic curvature (c_0^{-1} = 3–100 nm); 3), protein-protein interaction (0–1 amu (nm/ps)^2); and 4), the level of membrane stiffening induced by the protein (η = 0–2.5), where membrane was stiffened according to $\kappa(\varphi_B) = \kappa(1 - \eta\varphi_{B,0})$.To quantify the time progress of the transformation and structurally

define its final configurations, we defined an order parameter T_u (level of tubulation (Eq. 3)). This parameter borrows from the theory of nematic crystals by making use of the orientation of the dipoles, superimposed on the membrane quasiparticles that describe the direction of the bilayer. It measures the extent to which the structure of the membrane has turned from a nontubulated into a tubulated state, on a scale from 0 to 1.

$$T_u = \frac{1}{N}\sum_{i=1}^{N}\frac{1}{N_{\text{cut}}}\sum_{j=1,r_{i,j}<r_{\text{cut}}}^{N_{\text{cut}}}\frac{3\left(\mathbf{\Omega}_i \cdot \mathbf{\Omega}_j\right)^2 - 1}{2} \qquad (3)$$

Here, $\mathbf{\Omega}$ is a vector normal to the membrane, N represents the number of quasiparticles, r is the distance between particles, i and j denote the particles, and the subscript cut denotes values within a designated cutoff distance.

In the tested range of mechanical variables, we identified three distinct equilibrium states of the vesicle: 1), buckling and bud formations; 2) irregular reticulation; and 3), reticulation. Fig. 4 depicts a phase diagram relating the mechanical properties of the membrane and the protein to the morphological consequences of (N-)BAR protein binding. Small values of the order parameter ($T_u < 0.3$) represent vesicle budding (Fig. 4, *squares*). Intermediate values of the order parameter ($T_u \sim 0.7$) represent irregular reticular vesicles (Fig. 4, *diamonds*). Structurally, these vesicles contain irregularly shaped tubules, a smaller number of junctions (usually half that of fully reticular vesicles) and exhibit slower remodeling dynamics (by a factor of 2–5).

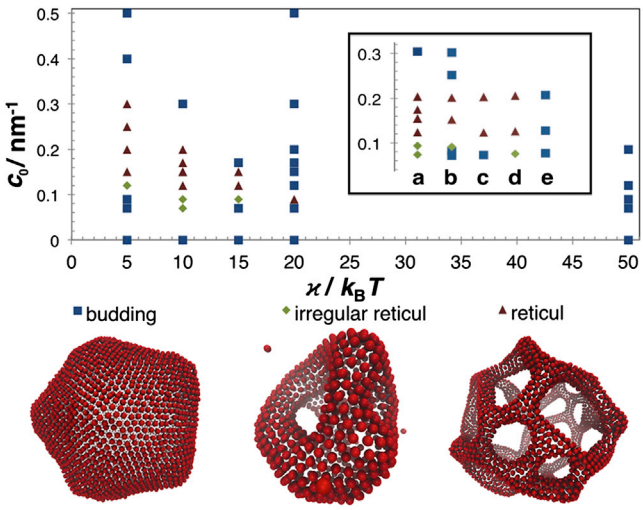

FIGURE 4 Phase diagram for the topological transformation of 250 nm vesicles. In the diagram, each symbol (*square*, *diamond*, and *triangle*) represents an independent mesoscopic simulation for which the equilibrium structure (*budding*, *irregular reticul*, *reticul*) was determined based on the value of T_u. κ denotes bending stiffness and c_0^{-1} intrinsic curvature. Boxed is the comparison at $\kappa = 10\ k_BT$ (*lane a*) for other tested parameters: 100 nm vesicle (*lane b*), oligomerization energy from 0 to 1 amu (nm/ps)^2 (*lane c*), no membrane stiffening ($\eta = 0$) (*lane d*), and strong membrane stiffening ($\eta = 2.5$) (*lane e*).

Finally, large values of the tubulation order parameter ($T_u \sim 0.85$) represent a fully reticular vesicle (Fig. 4, *triangles*). Fig. S3 depicts the evolution of the order parameter for three distinct vesicle states. Fully reticular structures are prevalent at values of bending stiffness typical for most lipid bilayers (5–15 k_BT). As the bending stiffness increases, the occurrence of remodeling was significantly decreased, with no remodeling observed above $k = 20\ k_BT$. Irregular reticular structures are observed only in a small part of the phase diagram when the interacting particles (proteins) do not have a large enough intrinsic curvature (c_0^{-1}) to cause a fully reticular structure. Higher intrinsic curvatures represent BAR proteins with more curved shape and/or higher number of amphipathic helices. As the bending stiffness decreases, higher intrinsic curvatures are required for topological transformation (0.15 nm^{-1} threshold for 5 k_BT, 0.12 nm^{-1} for 10 k_BT, and 0.09 nm^{-1} for 20 k_BT). These results complement our assumption that a moderate stiffening of the membrane aids in the topological transformation. On the other hand, it is also difficult to induce curvature in membranes that are too stiff. The inset in Fig. 4 (*lane e*) confirms that very high local stiffening precludes the formation of reticular structures. At high intrinsic curvatures, the topological transformation is also prevented. Based on the rate at which the protein concentration field variable evolves, an increase in intrinsic curvature slows down the binding of the protein (Fig. 4). This feature arises because the model assumes that proteins bind by coupling to local curvature of the membrane. Curvature sensing and sorting has been well described for N-BAR and F-BAR proteins in fluorescence microscopy experiments (17,45). Even in the absence of such interactions, the intrinsic curvatures beyond 0.4 nm^{-1} (radius $<$ 2.5 nm) are smaller than the bilayer thickness itself and would act on completely different scales. As a consequence, in this region of the phase space, only budding is observed, as a consequence of low-density binding and nonspecific interactions with the membrane. Taken together, topological transformations of lipid vesicles take place in a very narrow range of structural and mechanical parameters of the membrane and its interacting proteins. For most experimental lipid membranes, we expect the formation of the tubular network by proteins that induce spontaneous curvatures on the order of 0.12–0.20 nm^{-1}, values typical for N-BAR proteins. Considering the minimal parameterization of the protein in our mesoscopic simulation, the phase diagram indicates that membrane reticular structures could be engineered with high-affinity particles exhibiting the same range of intrinsic curvatures. We hope our work can inspire research in that direction.

CONCLUSIONS

One of the greatest feats that a eukaryotic cell can perform is the formation and maintenance of specialized membranous

structures. Many organelles and cellular structures contain highly reticular membrane segments, including the trans-Golgi network, the endoplasmic reticulum, and the transverse tubular system in the muscle cell (1). The formation of T-tubules, for example, requires amphiphysin, implicating N-BAR proteins in this process. It is becoming increasingly clear that these proteins have a diverse set of membrane remodeling capabilities, and our study points to their potential key role in forming and maintaining complex cellular structures. In these processes, a precise, and most likely protein-controlled, scission of the membrane would be required to prevent an uncontrolled influx of solutes into the cell. Our study demonstrates that the interaction of lipid vesicles and the N-BAR domains of endophilin present a minimal system to create complex reticular morphologies as found in living cells. We show that high-density surface binding, facilitated by large local protein concentrations and elevated membrane charge, are prerequisites for transforming a vesicle into a tubular network. Highly anisotropic interactions between N-BAR proteins and the membrane drive protein aggregation, generating the initial curvature of the membrane. Local stiffening occurs as a result of protein binding and the significantly decreased mobility of lipids in the necks of membrane buds. As more proteins bind, the excess adhesive energy, combined with this local stiffening, causes the breaking of the bilayer topology. Both simulations and electron tomograms indicate that a preformed nematogenic phase of N-BAR proteins drives the subsequent tubulation and the stabilization of tubular structures. It is possible that these ordered assemblies are the actual deployable units for tubule formation in cells. Our hypothesis aligns well with the possibility that N-BAR proteins form linear aggregates before curvature generation. These linear aggregates could serve as nucleation sites for the formation of nematogenic constructs at much higher concentrations. Finally, our study adds to the recent discovery of N-BAR domains as being potential fissiogenic proteins (15). As such, they are able to penetrate and reseal the membrane, a prerequisite for the formation of a multitude of vital cellular structures.

SUPPORTING MATERIAL

Three figures and one table are available at http://www.biophysj.org/biophysj/supplemental/S0006-3495(13)00748-0.

We thank Marissa Saunders for the critical reading of the manuscript.

We acknowledge the support of the National Institutes of Health (NIH grant numbers GM063796 to GAV and GM094479 to VMU). Research in the Marlovits laboratory is supported by IMP and IMBA, and through a grant by Zentrum für Innovation and Technology (ZIT), Center for Molecular and Cellular Nanostructure (CMCN Vienna). We thank the National Science Foundation for providing computational resources through XSEDE (grant number TG-MCA94P017) on the Kraken supercomputer.

REFERENCES

1. Alberts, B. 2002. Molecular Biology of the Cell, 4th ed. Garland Science, New York.
2. Lipowsky, R. 1991. The conformation of membranes. *Nature.* 349: 475–481.
3. McMahon, H. T., and J. L. Gallop. 2005. Membrane curvature and mechanisms of dynamic cell membrane remodelling. *Nature.* 438: 590–596.
4. Ren, G., P. Vajjhala, …, A. L. Munn. 2006. The BAR domain proteins: molding membranes in fission, fusion, and phagy. *Microbiol. Mol. Biol. Rev.* 70:37–120.
5. Mim, C., and V. M. Unger. 2012. Membrane curvature and its generation by BAR proteins. *Trends Biochem. Sci.* 37:526–533.
6. Qualmann, B., D. Koch, and M. M. Kessels. 2011. Let's go bananas: revisiting the endocytic BAR code. *EMBO J.* 30:3501–3515.
7. Frost, A., V. M. Unger, and P. De Camilli. 2009. The BAR domain superfamily: membrane-molding macromolecules. *Cell.* 137:191–196.
8. Peter, B. J., H. M. Kent, …, H. T. McMahon. 2004. BAR domains as sensors of membrane curvature: the amphiphysin BAR structure. *Science.* 303:495–499.
9. Mim, C., H. Cui, …, V. M. Unger. 2012. Structural basis of membrane bending by the N-BAR protein endophilin. *Cell.* 149:137–145.
10. Lee, E., M. Marcucci, …, P. De Camilli. 2002. Amphiphysin 2 (Bin1) and T-tubule biogenesis in muscle. *Science.* 297:1193–1196.
11. Frost, A., R. Perera, …, V. M. Unger. 2008. Structural basis of membrane invagination by F-BAR domains. *Cell.* 132:807–817.
12. van Weering, J. R., R. B. Sessions, …, P. J. Cullen. 2012. Molecular basis for SNX-BAR-mediated assembly of distinct endosomal sorting tubules. *EMBO J.* 31:4466–4480.
13. Mattila, P. K., A. Pykäläinen, …, P. Lappalainen. 2007. Missing-in-metastasis and IRSp53 deform PI(4,5)P2-rich membranes by an inverse BAR domain-like mechanism. *J. Cell Biol.* 176:953–964.
14. Campelo, F., H. T. McMahon, and M. M. Kozlov. 2008. The hydrophobic insertion mechanism of membrane curvature generation by proteins. *Biophys. J.* 95:2325–2339.
15. Boucrot, E., A. Pick, …, M. M. Kozlov. 2012. Membrane fission is promoted by insertion of amphipathic helices and is restricted by crescent BAR domains. *Cell.* 149:124–136.
16. Wang, Q., M. V. Navarro, …, H. Sondermann. 2009. Molecular mechanism of membrane constriction and tubulation mediated by the F-BAR protein Pacsin/Syndapin. *Proc. Natl. Acad. Sci. USA.* 106:12700–12705.
17. Sorre, B., A. Callan-Jones, …, A. Roux. 2012. Nature of curvature coupling of amphiphysin with membranes depends on its bound density. *Proc. Natl. Acad. Sci. USA.* 109:173–178.
18. Ayton, G. S., and G. A. Voth. 2010. Multiscale simulation of protein mediated membrane remodeling. *Semin. Cell Dev. Biol.* 21:357–362.
19. Ayton, G. S., and G. A. Voth. 2009. Systematic multiscale simulation of membrane protein systems. *Curr. Opin. Struct. Biol.* 19:138–144.
20. Ayton, G. S., E. Lyman, …, G. A. Voth. 2009. New insights into BAR domain-induced membrane remodeling. *Biophys. J.* 97:1616–1625.
21. Ayton, G. S., J. L. McWhirter, and G. A. Voth. 2006. A second generation mesoscopic lipid bilayer model: connections to field-theory descriptions of membranes and nonlocal hydrodynamics. *J. Chem. Phys.* 124:64906.
22. Srivastava, A., and G. A. Voth. 2013. Hybrid approach for highly coarse-grained lipid bilayer models. *J. Chem. Theory Comput.* 9:750–765.
23. Noid, W. G., J. W. Chu, …, H. C. Andersen. 2008. The multiscale coarse-graining method. I. A rigorous bridge between atomistic and coarse-grained models. *J. Chem. Phys.* 128:244114.
24. Izvekov, S., and G. A. Voth. 2005. A multiscale coarse-graining method for biomolecular systems. *J. Phys. Chem. B.* 109:2469–2473.

25. Ayton, G. S., E. Lyman, and G. A. Voth. 2010. Hierarchical coarse-graining strategy for protein-membrane systems to access mesoscopic scales. *Faraday Discuss.* 144:347–357, discussion 445–381.

26. Lyman, E., H. S. Cui, and G. A. Voth. 2011. Reconstructing protein remodeled membranes in molecular detail from mesoscopic models. *Phys. Chem. Chem. Phys.* 13:10430–10436.

27. Plimpton, S. 1995. Fast parallel algorithms for short-range molecular-dynamics. *J. Comput. Phys.* 117:1–19.

28. Fraternali, F., C. D. Lorenz, and G. Marcelli. 2012. On the estimation of the curvatures and bending rigidity of membrane networks via a local maximum-entropy approach. *J. Comput. Phys.* 231:528–540.

29. Hoover, W. G., and C. G. Hoover. 2003. Links between microscopic and macroscopic fluid mechanics. *Mol. Phys.* 101:1559–1573.

30. McWhirter, J. L., G. Ayton, and G. A. Voth. 2004. Coupling field theory with mesoscopic dynamical simulations of multicomponent lipid bilayers. *Biophys. J.* 87:3242–3263.

31. Suloway, C., J. Pulokas, …, B. Carragher. 2005. Automated molecular microscopy: the new Leginon system. *J. Struct. Biol.* 151:41–60.

32. Kremer, J. R., D. N. Mastronarde, and J. R. McIntosh. 1996. Computer visualization of three-dimensional image data using IMOD. *J. Struct. Biol.* 116:71–76.

33. Schneider, C. A., W. S. Rasband, and K. W. Eliceiri. 2012. NIH Image to ImageJ: 25 years of image analysis. *Nat. Methods.* 9:671–675.

34. Khelashvili, G., D. Harries, and H. Weinstein. 2009. Modeling membrane deformations and lipid demixing upon protein-membrane interaction: the BAR dimer adsorption. *Biophys. J.* 97:1626–1635.

35. Aranda-Espinoza, H., Y. Chen, …, D. A. Weitz. 1999. Electrostatic repulsion of positively charged vesicles and negatively charged objects. *Science.* 285:394–397.

36. Chen, Y., and P. Nelson. 2000. Charge-reversal instability in mixed bilayer vesicles. *Phys. Rev. E Stat. Phys. Plasmas Fluids Relat. Interdiscip. Topics.* 62:2608–2619.

37. Sarić, A., and A. Cacciuto. 2012. Fluid membranes can drive linear aggregation of adsorbed spherical nanoparticles. *Phys. Rev. Lett.* 108: 118101.

38. Ramakrishnan, N., P. B. Sunil Kumar, and J. H. Ipsen. 2013. Membrane-mediated aggregation of curvature-inducing nematogens and membrane tubulation. *Biophys. J.* 104:1018–1028.

39. Cui, H., C. Mim, …, G. A. Voth. 2013. Understanding the role of amphipathic helices in N-BAR domain driven membrane remodeling. *Biophys. J.* 104:404–411.

40. Axelrod, D. 1983. Lateral motion of membrane proteins and biological function. *J. Membr. Biol.* 75:1–10.

41. Doeven, M. K., J. H. Folgering, …, B. Poolman. 2005. Distribution, lateral mobility and function of membrane proteins incorporated into giant unilamellar vesicles. *Biophys. J.* 88:1134–1142.

42. Domanov, Y. A., S. Aimon, …, P. Bassereau. 2011. Mobility in geometrically confined membranes. *Proc. Natl. Acad. Sci. USA.* 108:12605–12610.

43. Frick, M., K. Schmidt, and B. J. Nichols. 2007. Modulation of lateral diffusion in the plasma membrane by protein density. *Curr. Biol.* 17:462–467.

44. Horton, M. R., F. Hofling, …, T. Franosch. 2010. Development of anomalous diffusion among crowding proteins. *Soft Matter.* 6:2648–2656.

45. Ramesh, P., Y. F. Baroji, …, P. M. Bendix. 2013. FBAR syndapin 1 recognizes and stabilizes highly curved tubular membranes in a concentration dependent manner. *Sci. Rep.* 3:1565.